Types of the jump phenomenon in the angular dependence of the noncollinear exchange bias*

Yang Hong-Ping(杨红萍) and Bai Yu-Hao(白宇浩)†

College of Physics and Electronic Information, Shanxi Normal University, Linfen 041004, *China*

(Received 6 September 2013; revised manuscript received 24 December 2013; published online 20 April 2014)

Based on the principle of minimal energy and the coherent rotation model, two types of the jump phenomena, complete and incomplete jump phenomenon, are proved to exist in the angular dependence of the exchange bias with noncollinear unidirectional and uniaxial anisotropies. It is found that the transition between complete and incomplete jump phenomena occurs on condition that the exchange-coupling constant exceeds a critical value. Additionally, two different modes of the magnetization rotation, the whole-plane rotation, and the half-plane rotation are present in the magnetization reversal process, and they are dependent on the direction of the external field. Furthermore, the equations of the critical angle, at which orientation the exchange bias field reaches a maximum value and the coercivity disappears, are also derived in this paper. The numerical calculations in this paper are consistent with the relevant experimental observations, indicating that our method to study the angular dependence of the exchange bias as well as the magnetization reversal behaviors is valid. Our discussion about the jump phenomenon, the critical angle, and the modes of the magnetization reversal can explain the observed differences in results between different experiments.

Keywords: jump phenomenon, angular dependence of the exchange bias, mode of the magnetization reversal, critical angle

PACS: 75.30.Gw, 75.60.Jk, 75.70.−i **DOI:** 10.1088/1674-1056/23/6/067503

1. Introduction

Exchange bias (EB) means a shift of the hysteresis loop for a ferromagnetic (FM) system or an antiferromagnetic (AFM) system, such as FM/AFM bilayers, along the magnetic field axis below the blocking temperature. This effect has been widely applied in magnetoresistance or spintronic devices.[1,2] Although EB has been extensively investigated for more than fifty years, its characteristics, such as coercivity enhancement, training effect, and asymmetric magnetization reversal, have not been understood satisfactorily. For reviews concerning both theories and experiments, readers may refer to Refs. [3]–[7].

The angular dependence of exchange bias (ADEB) is an important subject in the investigation of the exchange bias effect, which needs to know the exchange bias field $H_{\rm EB}$ and the coercivity $H_{\rm C}$, defined respectively as the shift and half-width of the hysteresis loop, each as a function of the orientation of external field, i.e., $H_{\rm EB}(\theta_{\rm H})$ and $H_{\rm C}(\theta_{\rm H})$ curves. ADEB is very informative to understand the nature of exchange bias effect, and it is also useful in providing an independent test for the validity of the theoretical models on the exchange bias.[8] On the other hand, the investigation of the ADEB is also valuable to achieve the maximal exchange bias field, maximal or minimal coercivity by tuning the orientation of the external field, which is technologically important in designing the magnetoresistance or spintronic devices.

Recently, it has been confirmed experimentally and theoretically that $H_{\rm EB}$ and $H_{\rm C}$ can display a jump phenomenon[9–17] in the ADEB, which cannot be described by cosine series expansion as done in the initial investigation.[8] This jump phenomenon has been found in both collinear[9–12] and noncollinear[13–17] exchange bias. The collinear exchange bias means that the orientation of the uniaxial anisotropy is parallel to the unidirectional anisotropy. On the contrary, a configuration of misalignment between unidirectional and uniaxial anisotropy axes can be present in the noncollinear exchange bias, which can be established either intrinsically by interfacial spin frustration[18–20] or extrinsically by a special field cooling procedure,[13,17] ion irradiation technique[21] or system for preparing the FM/AFM by the oblique sputtering deposition.[22]

For the collinear exchange bias, it is found that $H_{\rm EB}$ reaches its maximum, meanwhile $H_{\rm C}$ vanishes suddenly at the jumping points, which are defined as the intrinsic hard axes in Bai *et al.*'s work.[12] This type of the jump phenomenon has been named complete jump phenomenon in their work. Actually, the same feature has also been discovered by Liedke *et al.*[14] in the ADEB of NiFe/FeMn bilayers with noncollinear uniaxial and unidirectional anisotropies. Recently, Jiménez *et al.*[17] have also studied the ADEB of noncollinear exchange bias in Co/IrMn bilayers. The jump phenomenon is still present in the ADEB, whereas $H_{\rm EB}$ does not reach a max-

*Project supported by the Fundamental Research Foundation of Shanxi Province, China (Grant No. 2013021010-3) and the Natural Science Foundation of Shanxi Normal University, China (Grant No. 872014).

†Corresponding author. E-mail: phlyr@scut.edu.cn

© 2014 Chinese Physical Society and IOP Publishing Ltd

imum, moreover H_C does not disappear at the jumping points. The critical angle, where H_{EB} achieves the maximum and H_C starts to disappear, has been observed in the ADEB after the presence of the jump phenomenon.[17] This feature is similar to that of the incomplete jump phenomenon, which has also been proposed by Bai *et al.*[12] in the ADEB of the collinear exchange bias.

Based on the above experimental observations, a conclusion can be made that two different types of the jump phenomena, complete and incomplete jump phenomena, can also exist in the ADEB of the noncollinear exchange bias, though they manifest themselves in very different manners for different materials.[14,17] However, these features of the ADEB have not been explained by these authors. Although the jump phenomenon shown in the ADEB of the noncollinear exchange bias has been explained by Bai *et al.*,[15,16] the types of the jump phenomena were not emphasized in their work.

The intent of this study is to explain the complete and incomplete jump phenomena shown in the ADEB of the noncollinear exchange bias, which is useful for a better understanding of the ADEBs measured in different systems. By analyzing the magnetization reversal processes, the physical conditions of the transition between two types of the jump phenomena are obtained. Additionally, the critical angle and the mode of the magnetization reversal are also studied in this paper.

2. Theoretical model

The free energy per unit area of the FM /AFM bilayer can be expressed as[15,16,23]

$$E = K_F t_F \sin^2\theta_F - J_E \cos(\alpha - \theta_F) - HM_F t_F \cos(\theta_H - \theta_F). \quad (1)$$

On the right-hand side of Eq. (1), the first term represents the uniaxial anisotropy energy, in which K_F is the anisotropy constant and t_F is the thickness of the ferromagnetic material, and θ_F is the angle of the ferromagnetic magnetization M_F with respect to the easy axis of the uniaxial anisotropy which is defined as x axis for simplicity; the second term is the exchange anisotropy energy characterized by the exchange coupling constant J_E and its relative orientation α with respect to the uniaxial anisotropy axis. The ferromagnetic coupling is assumed to exist between the spins of the FM/AFM interfaces,which means $J_E > 0$, and the hysteresis loop with a negative shift will be observed when the external field is applied along the orientation of the cooling field, i.e., the easy axis of the unidirectional anisotropy; the last term corresponds to the Zeeman energy, in which H and θ_H denote respectively the magnitude and orientation of the external field. All the angles, θ_H, θ_F, and α, are counted clockwise from the positive x semiaxis.

According to the method of monostable and bistable states proposed by Bai *et al.*,[12] we first discuss the initial magnetization state of the system (the state when the external field is absent). Using Jiménez *et al.*'s parameters,[17] $J = K_E/2K_U = 8.1/5.2 \approx 1.5577$, $\alpha = 20^\circ$ in the calculations, where $J = J_E/2K_F t_F$ is defined as the reduced exchange-coupling constant. Figure 1(a) shows the dependences of the normalized energy $E/2K_F t_F$ on the ferromagnetic magnetization orientation θ_F in the initial magnetization state. Because only one energy minimum θ_{F1} together with one energy maximum θ_{F2} is shown in the energy spectrum, the system will be in the monostable state. The parameters $J = 0.65$ and $\alpha = 20^\circ$ are chosen in the calculations in order to compare the results with the parameters $J = 1.5577$ and $\alpha = 20^\circ$. The orientations of θ_{F1} and θ_{F2} are respectively defined as the intrinsic easy and hard axes.[12] The values of θ_{F1} and θ_{F2} can be obtained from the equilibrium condition: $\partial E(H=0)/\partial\theta_F = 0$, which can be given by

$$\frac{1}{2}\sin 2\theta_F - J\sin(\alpha - \theta_F) = 0. \quad (2)$$

For $J = 1.5577$ and $\alpha = 20^\circ$, $\theta_{F1} = 12.3133^\circ$ and $\theta_{F2} = 218.1751^\circ$, respectively for the intrinsic easy and hard axes, can be obtained by solving Eq. (2). For the case of $J = 0.65$ and $\alpha = 20^\circ$, the calculated results are $\theta_{F1} = 7.904^\circ$ and $\theta_{F2} = 240.8643^\circ$. The positions of the intrinsic easy and hard axes together with their perpendicular orientations divide the directions of the external field into several angular regions, which can be used to analyze the magnetization reversal processes conveniently.[12,15,16] The schematic diagram of the positions of θ_{F1} and θ_{F2} together with the angular regions are shown in Fig. 1(b).

The coherent rotation model,[24] although the effect of the microstructure such as grain size, interface roughness or domains is not taken into account in the magnetization process, has been proved to be an effective method to describe the magnetization reversal in many exchange-coupled systems.[9–17,25,26] Likewise, this model is also used to analyze the magnetization reversal processes in this paper. As complete and incomplete jump phenomenon in the ADEB can be discriminated by the different features of the exchange bias at the orientation of the intrinsic hard axis,[12] the magnetization reversal processes, when the external field is applied around the intrinsic hard axis $\theta_{F2} - 180^\circ$, should be discussed. Because $\theta_{F2} - 180^\circ$ is the boundary of the angular regions 2 and 3 as depicted in Fig. 1(b), we must analyze the magnetization reversal processes in these two angular regions. M_F stays at the position of θ_{F1} in the initial magnetization state. The perfect-delay convention,[27] which means that M_F remains in a local-energy minimum until the energy barrier between the local and global energy minimum vanishes, is used in the numerical calculations. The exchange bias field H_{EB} and the coercivity H_C

can be deduced from the relation $H_{EB} = (H_{CR} + H_{CL})/2$ and $H_C = (H_{CR} - H_{CL})/2$, where H_{CL} and H_{CR} are the coercive fields for the descending and ascending branches of the hysteresis loop, respectively.

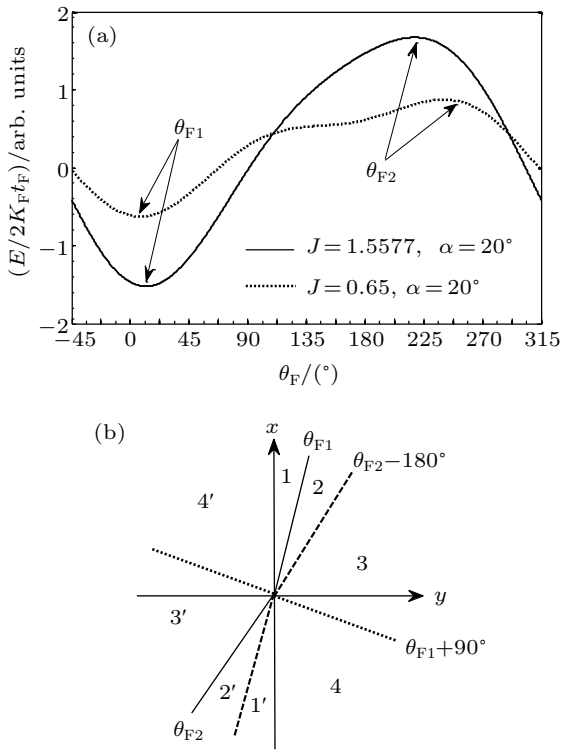


Fig. 1. (a) Values of normalized energy $E/2K_Ft_F$ each as a function of the ferromagnetic magnetization orientation θ_F when the external field H is absent. The parameters are taken as $J = 0.65$, $J = 1.5577$, and $\alpha = 20°$ in the numerical calculations. (b) Schematic diagram for the positions of the intrinsic easy axis θ_{F1}, the intrinsic hard axis θ_{F2}, and the corresponding angular regions of the external field.

Figure 2(a) shows the rotation of M_F when the orientation of the external field is within the scope of the angular region 2, i.e., $\theta_{F1} \le \theta_H < \theta_{F2} - 180°$. The coercive field H_{CL} appears when H reverses its direction and increases from zero to the negative saturation. Considering the torque exerted on M_F by H, M_F rotates away from θ_{F1} towards the opposite orientation of H in an anticlockwise sense to diminish the Zeeman energy. The determined formula of H_{CL} is given by[16]

$$\begin{aligned}
&\frac{E}{2K_Ft_F} = \frac{1}{2}\sin^2(\theta_{F1}-\theta) - J\cos(\alpha-\theta_{F1}+\theta)\\
&\qquad\qquad -h\cos(180°-\theta_H+\theta_{F1}-\theta),\\
&-\frac{1}{2}\sin 2(\theta_{F1}-\theta) + J\sin(\alpha-\theta_{F1}+\theta)\\
&-h\sin(180°-\theta_H+\theta_{F1}-\theta) = 0,\\
&\cos 2(\theta_{F1}-\theta) + J\cos(\alpha-\theta_{F1}+\theta)\\
&+h\cos(180°-\theta_H+\theta_{F1}-\theta) \ge 0,
\end{aligned} \tag{3a}$$

where θ is the angle between M_F and θ_{F1}; $h = H/H_A$ and $H_A = 2K_F/M_F$ are defined respectively as the normalized field and the uniaxial anisotropy field. Based on the method of the

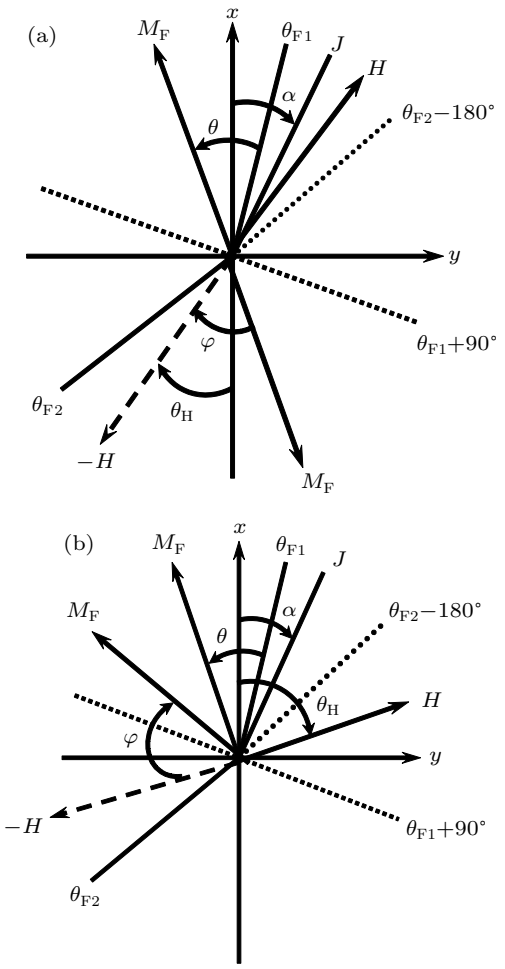


Fig. 2. Rotation of M_F in the magnetization reversal process for the angular regions $\theta_{F1} \le \theta_H < \theta_{F2} - 180°$ (a) and $\theta_{F2} - 180° \le \theta_H < \theta_{F1} + 90°$ (b). The dashed line with arrow represents the opposite orientation of the applied field H. θ and φ are the angles included between M_F and θ_{F1} and between M_F and $-H$ during the descending and ascending branches of the hysteresis loop, respectively.

geometrical asteroid solution of the coherent rotation model,[28] H_{CL} can be expressed as

$$H_{CL} = \begin{cases} H_{LS} \to (J\sin\alpha - h\sin\theta_H)^{2/3} + (J\cos\alpha - h\cos\theta_H)^{2/3} \\ \qquad = 1, \quad \text{for} \quad \theta_H \le \theta_H^*, \\ H_{90} = 0.5\sin 2\theta_H + J\cos(\theta_H - \alpha), \quad \text{for} \quad \theta_H > \theta_H^*, \end{cases} \tag{3b}$$

where H_{LS} is the switching field of the descending branch of the hysteresis loop. For $h = H_{LS}$, M_F will make an irreversible rotation from an orientation far away from the external field to another orientation close to the external field. The determined equation of H_{LS} can be derived from the conditions of $\partial(E/2K_Ft_F)/\partial\theta = 0$ and $\partial^2(E/2K_Ft_F)/\partial\theta^2 = 0$, which has been given by the first formula of Eq. (3b). On the other hand, if the perpendicular angle $\theta_{90} = 90° - \theta_H + \theta_{F1}$ is substituted into the first formula of Eq. (3a), the perpendicular field H_{90} can be derived. At H_{90}, M_F is expected to be perpendicular to the external field in the magnetization reversal process. The relevant equation of H_{90} is given by the second formula of Eq. (3b). Based on the perfect-delay convention, it is found

that θ_{90} starts to become a stable position of M_F until θ_H is above a critical value θ_H^*, which can be derived by substituting the condition $\theta_{90} = 90^\circ - \theta_H + \theta_{F1}$ into the characteristic equation $\partial^2(E/2K_F t_F)/\partial\theta^2 = 0$. The corresponding equation of θ_H^* can be written as

$$\cos 2\theta_H^* - J\sin(\theta_H^* - \alpha) = 0. \tag{3c}$$

Only if the condition of $\theta_H > \theta_H^*$ is satisfied, the perpendicular field H_{90} will be taken as the coercive field H_{CL}. Otherwise, the switching field H_{LS} will replace H_{90}, serving as H_{CL} under the condition of $\theta_H \le \theta_H^*$.

When H increases from zero to the negative saturation, M_F is capable of passing through the intrinsic hard axis θ_{F2} as shown in Fig. 2(a). Hence, when H releases itself from the negative saturation to zero, instead of rotating back to the position of θ_{F1} from the negative orientation of H in a clockwise sense, M_F will continue its anticlockwise rotation from $-H$ towards θ_{F1}. The other coercive field H_{CR} occurs at this magnetization stage and the determined formula is given by[16]

$$\begin{aligned}
&\frac{E}{2K_F t_F} = \frac{1}{2}\sin^2(180^\circ + \theta_H - \varphi) - J\cos(180^\circ + \theta_H - \alpha - \varphi) \\
&\qquad - h\cos\varphi, \\
&-\frac{1}{2}\sin 2(180^\circ + \theta_H - \varphi) - J\sin(180^\circ + \theta_H - \alpha - \varphi) \\
&\qquad + h\sin\varphi = 0, \\
&\cos 2(180^\circ + \theta_H - \varphi) + J\cos(180^\circ + \theta_H - \alpha - \varphi) \\
&\qquad + h\cos\varphi \ge 0,
\end{aligned} \tag{4a}$$

where φ is the angle included between M_F and $-H$ as illustrated in Fig. 2(a). The analytical expression of H_{CR} can also be gained by the method of the geometrical asteroid solution of the coherent rotation model, which can be written as

$$H_{CR} = \begin{cases} H_{RS} \to (J\sin\alpha - h\sin\theta_H)^{2/3} + (J\cos\alpha - h\cos\theta_H)^{2/3} \\ \qquad = 1, \quad \text{for} \quad \theta_H \le \theta_H', \\ H_{90} = -0.5\sin 2\theta_H + J\cos(\theta_H - \alpha), \quad \text{for} \quad \theta_H > \theta_H'. \end{cases} \tag{4b}$$

The critical angle θ_H' can be obtained from the relation $H_{RS} = H_{90}$, which can be expressed as

$$\begin{aligned}
&\left[\cos\theta_H'\left(J\sin\left(\theta_H' - \alpha\right) - \sin^2\theta_H'\right)\right]^{2/3} \\
&\qquad + \left[\sin\theta_H'\left(\cos^2\theta_H' + J\sin\left(\theta_H' - \alpha\right)\right)\right]^{2/3} = 1.
\end{aligned} \tag{4c}$$

Although the switching fields H_{LS} and H_{RS} have the same equation, which is expressed by the first formula of Eq. (3b) or Eq. (4b), they come from two different solutions of this transcendental equation actually. This result is caused by the effect of the unidirectional anisotropy on the broken symmetry of the initial uniaxial anisotropy,[26] and the equilibrium positions of M_F between the descending and the ascending branches of the hysteresis loop are not equivalent to each other any more. Consequently, two different switching fields H_{LS} and H_{RS} will appear in the above two magnetization stages.

The magnetization reversal processes for the angular region 3, i.e., $\theta_{F2} - 180^\circ \le \theta_H < \theta_{F1} + 90^\circ$, are indicated in Fig. 2(b). H_{CL} also occurs at the magnetization stage of H increasing from zero to the negative saturation, and the determined formula is the same as Eq. (3). Compared with the situation of the angular region 2, M_F cannot pass through the intrinsic hard axis θ_{F2} when H increases from zero to the negative saturation under the condition of $\theta_{F2} - 180^\circ \le \theta_H < \theta_{F1} + 90^\circ$. It induces a clockwise rotation of M_F from $-H$ toward θ_{F1} when H decreases from the negative saturation to zero. Accordingly, the determined formula of H_{CR} is different from the one of the angular region 2, which is expressed as[16]

$$\begin{aligned}
&\frac{E}{2K_F t_F} = \frac{1}{2}\sin^2(180^\circ + \theta_H + \varphi) - J\cos(180^\circ + \theta_H - \alpha + \varphi) \\
&\qquad - h\cos\varphi, \\
&\frac{1}{2}\sin 2(180^\circ + \theta_H + \varphi) + J\sin(180^\circ + \theta_H - \alpha + \varphi) \\
&\qquad + h\sin\varphi = 0, \\
&\cos 2(180^\circ + \theta_H + \varphi) + J\cos(180^\circ + \theta_H - \alpha + \varphi) \\
&\qquad + h\cos\varphi \ge 0.
\end{aligned} \tag{5a}$$

The expression of H_{CR} can also be written as

$$H_{CR} = \begin{cases} H_{RS} \to (J\sin\alpha - h\sin\theta_H)^{2/3} + (J\cos\alpha - h\cos\theta_H)^{2/3} \\ \qquad = 1, \quad \text{for} \quad \theta_H \le \theta_H'', \\ H_{90} = 0.5\sin 2\theta_H + J\cos(\theta_H - \alpha), \quad \text{for} \quad \theta_H > \theta_H''. \end{cases} \tag{5b}$$

The angle θ_H'' can be derived from the condition of $H_{RS} = H_{90}$ based on the perfect-delay convention, which can be written as

$$\begin{aligned}
&\left[\cos\theta_H''\left(J\sin\left(\theta_H'' - \alpha\right) + \sin^2\theta_H''\right)\right]^{2/3} \\
&\qquad + \left[\sin\theta_H''\left(\cos^2\theta_H'' - J\sin\left(\theta_H'' - \alpha\right)\right)\right]^{2/3} = 1.
\end{aligned} \tag{5c}$$

Considering that M_F rotates either in clockwise or in counterclockwise sense at the magnetization stage of releasing H from the negative saturation to zero, the determined formulas of H_{CR} are different in angular regions 2 and 3, which are given by Eq. (4) and Eq. (5), respectively. Consequently, H_{CR} is discontinuous at the boundary of two angular regions, i.e., $\theta_H = \theta_{F2} - 180^\circ$. However, H_{CL} is continuous at $\theta_{F2} - 180^\circ$ because of the same determined formula given by Eq. (3) in both angular regions 2 and 3. As a result, H_{EB} and H_C can make an abrupt change at $\theta_{F2} - 180^\circ$, which results in the presence of the jump phenomenon shown at $\theta_H = \theta_{F2} - 180^\circ$ in the

ADEB. Considering the symmetry, H_{CL} is discontinuous and H_{CR} is continuous at $\theta_H = \theta_{F2}$, which also leads to the jump phenomenon shown at $\theta_H = \theta_{F2}$ in the ADEB.

Furthermore, by analyzing the magnetization reversal process of the angular region 2, it can be found that the trace of M_F is of an anticlockwise rotation from the location of $+H$ to $-H$ in the descending branch of the hysteresis loop, and it is also of an anticlockwise rotation from $-H$ to $+H$ in the ascending branch of the hysteresis loop. This means that M_F experiences a whole-plane rotation in the magnetization reversal process. However, if M_F does not cross the intrinsic hard axis θ_{F2} for the case of the angular region 3, the trace of M_F is of an anticlockwise rotation from $+H$ to $-H$ in the descending branch of the hysteresis loop, while it is of a clockwise rotation from $-H$ to $+H$ in the ascending branch of the hysteresis loop. It means the magnetization reversal will exhibit a half-plane rotation mode. Additionally, the conclusion that the half-plane rotation mode appears in angular regions 1 and 4 can also be deduced from the similar analyses of the magnetization reversal. The different modes of the magnetization reversal can be revealed by measuring the perpendicular hysteresis loop $M_T(H)$, which has been reported in many experiments.[13,17,20,26,28] Although the magnetization reversal can be well described with the coherent rotation model in these studies, the mechanisms of two modes of the magnetization reversal are not always explained.

3. Numerical results and discussion

3.1. Hysteresis loops and the mode of the magnetization reversal

Based on the analysis of the coercive fields, the hysteresis loops including both the parallel component M_L and the perpendicular component M_T to the external field can be calculated. The representative hysteresis loops for each angular region are summarized in Fig. 3. When the magnetization reversal process displays the whole-plane rotation mode for the angular region 2, it can be seen from Fig. 3(c) that M_T exhibits both positive and negative signs in the hysteresis loops of $M_T(H)$. On the contrary, M_T always displays the same sign when the half-plane rotation mode occurs in angular regions 1, 3, and 4, i.e., either positive or negative sign is shown in an $M_T(H)$ curve. This extraordinary feature that M_T shows the same or different signs in an $M_T(H)$ curve has been observed in many experiments,[13,17,20,26,28] and it can be explained as the different modes of the magnetization reversal shown in different angular regions.

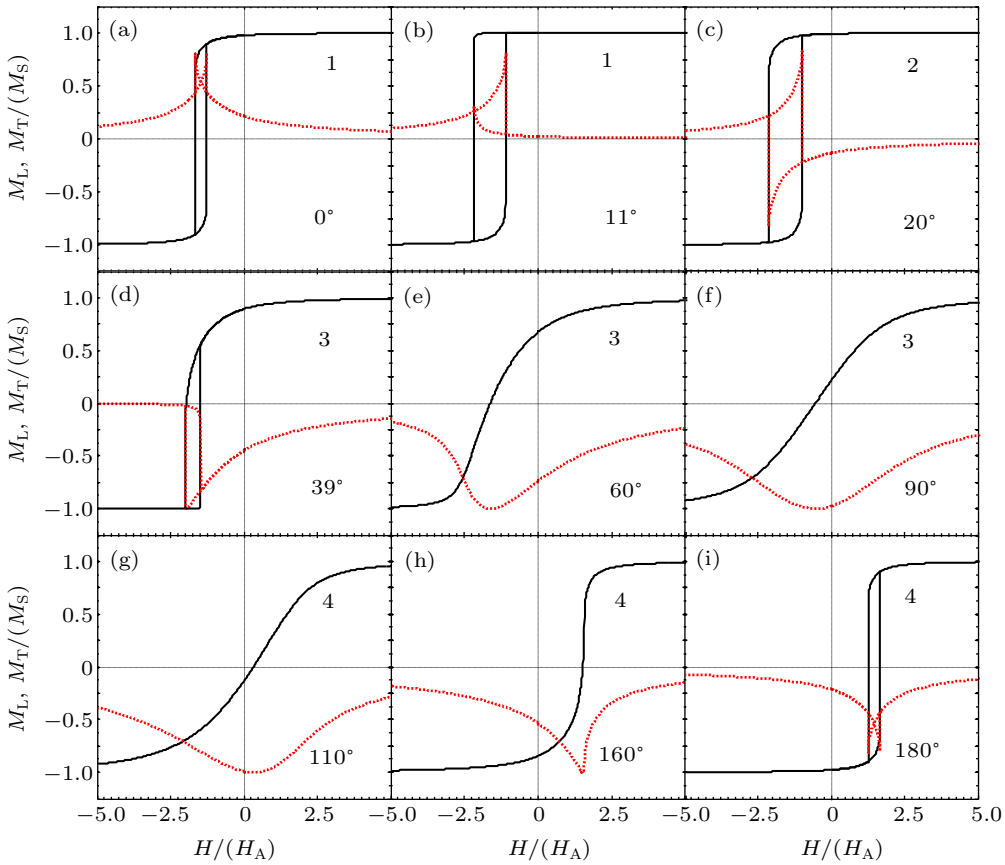


Fig. 3. (color online) The representative hysteresis loops in each angular region with the parameters $J = 1.5577$, $\alpha = 20°$. The parallel (M_L) and perpendicular components (M_T) of M_F to the applied field H are indicated by the solid and dashed lines, respectively. The orientations of the external field as well as the corresponding angular regions are shown by the numbers located in the right upper and nether corners, respectively.

It is instructive to compare our theoretical results with Jiménez *et al.*'s experimental results.[17] It should be noticed that the reference axis of θ_H in our paper is different from that in Jiménez *et al.*'s work. The orientations of the applied field α_H in their paper were counted counterclockwise from the orientation of the cooling field direction, i.e., $\theta_H = 20^\circ$ in our work, which coincides with the easy axis of the unidirectional anisotropy and indicates that $\theta_H = 20^\circ - \alpha_H$. For $J = 1.5577$ and $\alpha = 20^\circ$, the range of angular region 2 can be deduced from Eq. (2), and the calculated result is from $\theta_H = \theta_{F1} = 12.3133^\circ$ to $\theta_H = \theta_{F2} - 180^\circ = 38.1751^\circ$. It indicates that the angular range of the hysteresis loops showing the whole-plane-rotation mode is from $\alpha_H = -18.1751^\circ$ to $\alpha_H = 7.6867^\circ$. This angular range is asymmetric with respect to the unidirectional anisotropy axis, i.e., $\alpha_H = 0^\circ$ as pointed out in their paper.[17] The other orientations of the external field which do not belong to angular range 2 will show the hysteresis loops with half-plane rotation mode. Comparisons of hysteresis loop between theoretical and experimental modes are given in Table 1. The theoretical predictions are consistent with the experimental observations except for $\alpha_H = -18^\circ$, whose location is close to the left boundary of the angular region 2 ($\alpha_H = -18.1751^\circ$).[17] This inconsistency can be attributed to the error of the measurements.

Table 1. Comparisons between the theoretical results calculated by our approach and the experimental observations given by Jiménez *et al.*'s work. The orientation of the external field is denoted by θ_H in this paper, and by α_H in Jiménez *et al.*'s work, which gives the relation $\theta_H = 20^\circ - \alpha_H$ as explained in the text. The parameters in the calculations are taken to be $J = K_E/2K_U = 1.5577$ and $\alpha = 20^\circ$, which are the same as those used in Jiménez *et al.*'s work.

Comparison	Types of the hysteresis loop		Critical angle	Crossing angle
Jiménez *et al.*'s work	$\alpha_H = -18^\circ$	half-plane	$\alpha_H \approx -25^\circ$, $\alpha_H \approx +40^\circ$	$\alpha_H \approx -81^\circ$, $\alpha_H \approx +99^\circ$
	$\alpha_H = -13.5^\circ$:	whole-plane		
	$\alpha_H = -9^\circ$:	whole-plane		
	$\alpha_H = -4.5^\circ$:	whole-plane		
	$\alpha_H = +4.5^\circ$:	whole-plane		
	$\alpha_H = +9^\circ$:	half-plane		
	$\alpha_H = +13.5^\circ$:	half-plane		
	$\alpha_H = +18^\circ$:	half-plane		
This work	$\theta_H = 38^\circ$:	whole-plane	$\theta_{C1} = 43.1893^\circ$, $\alpha_H = -23.1893^\circ$	$\theta_H = 102.3133^\circ$, $\alpha_H = -82.3133^\circ$
	$\theta_H = 33.5^\circ$:	whole-plane	$\theta_C = -16.6115^\circ$, $\alpha_H = +36.6115^\circ$	$\theta_H = -77.6867^\circ$, $\alpha_H = +97.6867^\circ$
	$\theta_H = 29^\circ$:	whole-plane		
	$\theta_H = 24.5^\circ$:	whole-plane		
	$\theta_H = 15.5^\circ$:	whole-plane		
	$\theta_H = 11^\circ$:	half-plane		
	$\theta_H = 6.5^\circ$:	half-plane		
	$\theta_H = 2^\circ$:	half-plane		

3.2. Complete and incomplete jump phenomena in the ADEB

Figure 4 shows the calculated results of the ADEB. Two types of the jump phenomena are clearly seen in the figures. The complete jump phenomena are shown in Figs. 4(a), 4(c), and 4(d). H_{EB} reaches its maximum, and H_C vanishes at the jumping points of the intrinsic hard axis θ_{F2} or $\theta_{F2} - 180^\circ$. Only one critical angle θ_C appears in the ADEB, and it is located in angular region 4. The incomplete jump phenomenon can be observed in Fig. 4(b). Although H_{EB} and H_C each show a jump, H_{EB} does not reach the maximum, and H_C does not disappear at the jumping point of θ_{F2} or $\theta_{F2} - 180^\circ$. Two critical angles, θ_{C1} and θ_C, can be observed in the ADEB, which is different from the case of the complete jump phenomenon. No matter whether the complete jump phenomenon or the incomplete jump phenomenon is shown at the intrinsic hard axis, it is worth noting that H_C always reaches its maximum when the external field is applied along the intrinsic easy axis θ_{F1} or $\theta_{F1} + 180^\circ$. In addition, it can also be seen that the amplitudes of $H_{EB}(\theta_H)$ curves and the angular ranges of zero-coercivity of $H_C(\theta_H)$ curves are enlarged, while the amplitudes of $H_C(\theta_H)$ curves are gradually reduced when J increases from 0.65 to 1.5577 under the condition of $\alpha = 20^\circ$. It reflects the effect of the competition between unidirectional and uniaxial anisotropies on the exchange bias, i.e., the uniaxial anisotropy can be strongly weakened by a larger unidirectional anisotropy in an exchange-biased system.

As shown in Fig. 4(b), the critical angle θ_{C1}, at which orientation H_{EB} achieves its maximum and H_C disappears, can be observed after the appearance of the jump phenomenon. This result is also consistent with the experimental observation.[17] It indicates that θ_{C1} is greater than $\theta_{F2} - 180^\circ$, and θ_{C1} is located in angular region 3. Considering the observation that H_C disappears when the external field points along the orientation of θ_{C1}, the condition $H_{CL} = H_{CR}$ should be satisfied for $\theta_H = \theta_{C1}$. By combining Eqs. (3) and (5) under the condition of $H_{CL} = H_{CR}$, the determined equation of θ_{C1} can be derived. It is found that the value of θ''_H is larger than θ^*_H according to the numerical solution of the transcendental Eqs. (3c) and (5c). Consequently, $H_{CL} = H_{LS}$ or H_{90} and $H_{CR} = H_{RS}$ will occur

in the case of $\theta_H < \theta''_H$. Because the switching fields H_{LS} and H_{RS} as well as the perpendicular field H_{90} are not equal to each other as discussed in the above section, H_C always exists for $\theta_H < \theta''_H$ by the reason of $H_{CL} \neq H_{CR}$. On the contrary, for the $\theta_H > \theta''_H$ case, as pointed out in Eq. (3b), the relation $H_{CL} = H_{90}$ can be found for the reason of $\theta_H > \theta''_H > \theta^*_H$, and the relation $H_{CR} = H_{90}$ will be found according to the discussion in Eq. (5b). Therefore, the condition $H_{CL} = H_{CR} = H_{90}$ is satisfied in the case of $\theta_H > \theta''_H$, which leads to the disappearance of the coercivity accordingly. Consequently, the critical angle, where H_C starts to disappear in $H_C(\theta_H)$ curve, is the angle θ''_H, i.e., $\theta_{C1} = \theta''_H$.

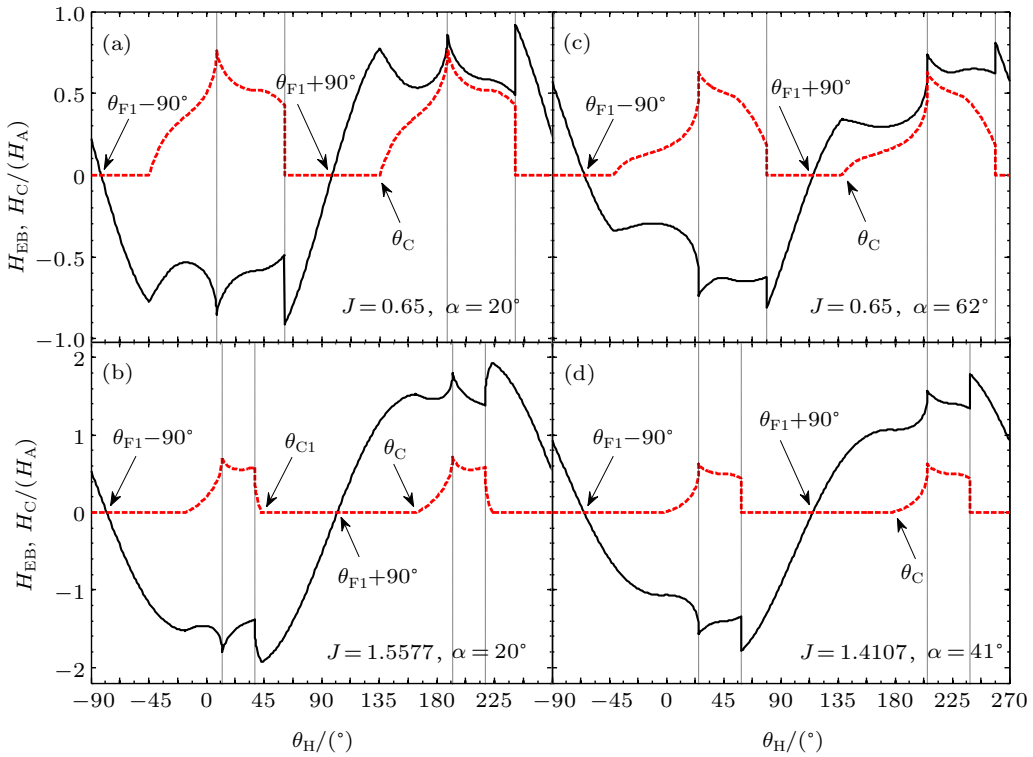


Fig. 4. (color online) Angular dependences of exchange bias field H_{EB} (solid lines) and the coercivity H_C (dashed lines). The applied field H is normalized by H_A. The positions of the intrinsic easy and hard axes θ_{F1}, $\theta_{F2} - 180°$, $\theta_{F1} + 180°$, and θ_{F2} are indicated by the vertical lines in sequence. The positions of the critical angles and the crossing angles are indicated by the arrows.

Furthermore, considering that θ_{C1} is located in the angular region 3, the condition $\theta_{C1} \geq \theta_{F2} - 180°$ must be satisfied. Substituting the critical condition $\theta_{C1} = \theta_{F2} - 180°$ into Eqs. (2) and (5c), one equation will be derived as follows:

$$\left[\sin\theta'_{C1}\cos\theta'_{C1}\left(\cos\theta'_{C1}+\sin\theta'_{C1}\right)\right]^{2/3} + \left[\sin\theta'_{C1}\cos\theta'_{C1}\left(\cos\theta'_{C1}-\sin\theta'_{C1}\right)\right]^{2/3} = 1, \quad (6)$$

where θ'_{C1} is a special value of the critical angle θ_{C1}. A meaningful solution $\theta'_{C1} = 58.2826°$ will be derived from the above equation. Substituting $\theta_{C1} = \theta_{F2} - 180°$ together with $\theta_{C1} = 58.2826°$ into Eq. (2), the expression about the critical exchange-coupling constant J_C can be derived as

$$J_C = \sin(58.2826°)\cdot\cos(58.2826°)/\sin(58.2826° - \alpha). \quad (7)$$

This simple expression is very useful to identify whether the complete or incomplete jump phenomenon will be observed in the ADEB. One will see that when J is above the critical value J_C under a fixed value of α, the incomplete jump phenomenon will be shown at the intrinsic hard axis. On the contrary, the complete jump phenomenon will be observed at the intrinsic hard axis under the condition of $J \leq J_C$. Taking $\alpha = 20°$ for example, the critical value $J_C \approx 0.7218$ can be derived from Eq. (7), hence the complete jump phenomenon will be shown at the intrinsic hard axis for $J = 1.5577$ and the incomplete jump phenomenon will be observed for $J = 0.65$ case. Additionally, it is also meaningful to make a comparison between our theoretic predictions and Liedke *et al.*'s experimental results.[14] Selecting $K_E = 7.9 \times 10^4$ erg/cm^2 (1 erg $= 10^{-7}$ J), $K_U = 2.8 \times 10^4$ erg/cm^2, and $\alpha = 41°$ as used in their paper, the critical exchange coupling constant $J_C = 1.5053$ can be deduced from Eq. (7) under the condition of $J = K_E/2K_U = 1.4107$ and $\alpha = 41°$. Therefore, the ADEB will exhibit a complete jump phenomenon at $\theta_{F2} - 180°$ or θ_{F2} for the reason of $J < J_C$. The corresponding results are shown in Fig. 4(d), which are in agreement with the experimental observations as seen in Fig. 3 of their paper.[14]

It should be stressed that a meaningless relation $J_C < 0$ will be derived from Eq. (7) for $\alpha > 58.2826°$, and it will disobey our supposition of ferromagnetic interfacial coupling. Consequently, two types of the jump phenomena shown at

the intrinsic hard axis will not occur unless the condition $\alpha \leq 58.2826^\circ$ is satisfied.

As mentioned above, the positions of the intrinsic easy and hard axes were determined by the parameters J and α. Under the condition of $\alpha \leq 58.2826^\circ$, it can be deduced from Eq. (2) that both the cases of $\theta_{F2} - 180^\circ > 58.2826^\circ$ and $\theta_{F2} - 180^\circ \leq 58.2826^\circ$ will be shown by tuning the parameter J. To be specific, when $J \geq J_C$, the case $\theta_{F2} - 180^\circ \leq 58.2826^\circ$ appears, and the incomplete jump phenomenon occurs at $\theta_{F2} - 180^\circ$. On the contrary, for $J < J_C$, $\theta_{F2} - 180^\circ > 58.2826^\circ$ is always present, which is accompanied with the complete jump phenomenon at $\theta_{F2} - 180^\circ$. As far as $\alpha > 58.2826^\circ$ is concerned, the relations $0^\circ < \theta_{F1} < \alpha$ and $180^\circ + \alpha < \theta_{F2} < 270^\circ$ will be derived from Eq. (2). Thus, the relation $\theta_{F2} - 180^\circ > 58.2826^\circ$ always holds due to $\theta_{F2} - 180^\circ > \alpha > 58.2826^\circ$. As a result, only the complete jump phenomenon should occur at $\theta_{F2} - 180^\circ$. The calculated ADEBs for $\alpha > 58.2826^\circ$ are shown in Fig. 4(c). The results about the type of the jump phenomenon at $\theta_{F2} - 180^\circ$ are consistent with the theoretical analyses. Consequently, the physical condition for the complete jump phenomenon is $\theta_{F2} - 180^\circ > 58.2826^\circ$ and it will be $\theta_{F2} - 180^\circ \leq 58.2826^\circ$ for the incomplete jump phenomenon.

Considering the fact that the parameters J and α determine directly the positions of the intrinsic hard axis, i.e., the value of $\theta_{F2} - 180^\circ$, which determines the type of the jump phenomenon directly as discussed above, a conclusion will be drawn that the complete or incomplete jump phenomenon in the ADEB is an intrinsic property of the exchange-coupled system, depending only on the relative magnitude and orientation between unidirectional and uniaxial anisotropies. A similar conclusion has been made in Bai *et al.*'s work for treating the ADEB of the collinear exchange bias,[12] but our methods in this paper are valid for analyzing the types of the jump phenomenon not only for the collinear exchange bias ($\alpha = 0^\circ$) but also for the noncollinear exchange bias ($\alpha \neq 0^\circ$). For example, if $\alpha = 0^\circ$ is substituted into Eq. (7), the critical exchange-coupling constant will be obtained by $J_C = \cos(58.2826^\circ) = \sqrt{1/2 - 1/2\sqrt{5}}$. This result coincides with the calculation in Bai *et al.*'s paper.[12]

As shown in Fig. 4, another critical angle θ_C is also observed in the ADEB, no matter whether the complete or incomplete jump phenomenon occurs at $\theta_{F2} - 180^\circ$. This critical angle appears at angular region 4, and the determined formula of θ_C has been given in Bai *et al.*'s work,[16] which is written as

$$AB - \left(\frac{1 - A^2 - B^2}{3}\right)^{3/2} = 0, \tag{8a}$$

where A and B are given by

$$\begin{cases} A = J\cos\alpha + h\cos\theta_C, \\ B = J\sin\theta_C + h\sin\theta_C, \\ h = -\sin\theta_C\cos\theta_C - J\cos(\theta_C - \alpha). \end{cases} \tag{8b}$$

The consistency between theoretical prediction and experimental observation about the critical angles is shown in Table 1.

Therefore, when the physical parameters J and α are known in a given exchange-biased system, the type of the jump phenomenon shown at the intrinsic hard axis can be inferred from Eq. (7). Then, the value of $\theta_{F2} - 180^\circ$ or θ_{C1}, at which orientation the maximal exchange bias field and the minimal coercivity ($H_C = 0$) occur, can be calculated according to the relevant equations, i.e., Eq. (2) or Eq. (5c). On the other hand, the largest coercivity always appears at the intrinsic easy axis. Hence, it will be an effective method to achieve the maximal exchange bias field as well as the maximal or minimal coercivity by aligning the external field along the corresponding orientations mentioned above. This idea is very important for the application of the exchange bias effect in the magnetoresistance or spintronic devices.

In addition, the crossing angles, where the $H_{EB}(\theta_H)$ curves intersect with the horizontal axis, can also be observed in Fig. 4. At these angles, the system shows no exchange bias field, i.e., $H_{EB} = 0$. Also, these crossing angles are the borderline between the positive values of H_{EB} and the negative one. To one's interest, these angles appear neither in the perpendicular orientation of the uniaxial anisotropy axis ($\theta_H = 90^\circ$) nor in the perpendicular orientation of the unidirectional anisotropy axis ($\theta_H = 90^\circ + \alpha$), it occurs in the perpendicular orientation of the intrinsic easy axis, i.e., $\theta_H = 90^\circ \pm \theta_{F1}$. Hence, the position of the intrinsic easy axis can be deduced from the intersection between the transverse axis and $H_{EB}(\theta_H)$ curve. It will be an effective method to gain the value of the intrinsic easy axis in a noncollinear exchange-biased system. The consistency between theoretical calculations and experimental observations about the crossing angles is shown in Table 1.

3.3. Measurement of the critical angle

Obviously, the critical angles θ_{C1} and θ_C as well as the intrinsic easy axis θ_{F1} and intrinsic hard axis $\theta_{F2} - 180^\circ$ will overlap each other in the ADEB if the angular deviations among these special angles are smaller. In that case, it will be difficult to observe the respective feature of these special angles in $H_{EB}(\theta_H)$ and $H_C(\theta_H)$ curves. When the complete jump phenomenon is present at the intrinsic hard axis, the angles θ_C, θ_{F1}, and $\theta_{F2} - 180^\circ$ do not overlap each other in the ADEB because their positions are located in different angular regions. However, when the incomplete jump phenomenon appears at $\theta_{F2} - 180^\circ$ under the condition of $\alpha \leq 58.2826^\circ$ and $J > J_C$, θ_{C1} will be present in the angular region 3 as discussed above. The position of θ_{C1} will be close to that of $\theta_{F2} - 180^\circ$ when the angular deviation between them is smaller, and their positions will overlap each other accordingly, resulting in an

indistinct observation of the critical angle θ_{C1}. Therefore, the calculations about the dependence of the angular deviation between $\theta_{F2} - 180^\circ$ and θ_{C1} on parameters J and α should be performed. The results of the numerical calculations are shown in Fig. 5.

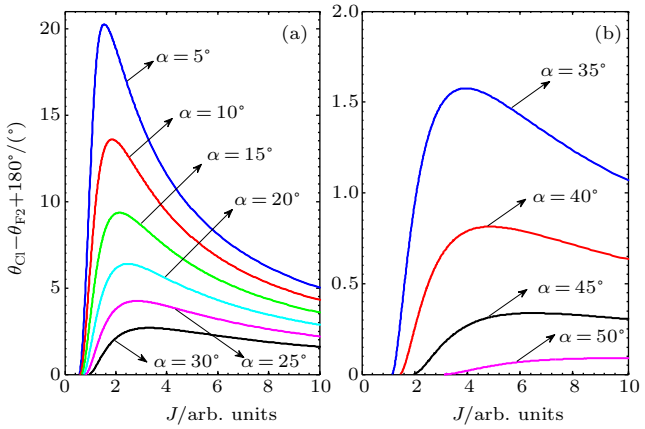


Fig. 5. (color online) Calculated values of angular deviation between the critical angle θ_{C1} and the intrinsic hard axis $\theta_{F2} - 180^\circ$ for (a) $0^\circ < \alpha \leq 30^\circ$ and (b) $30^\circ < \alpha < 58.2826^\circ$. The values of the noncollinear angles α are arrowed in the figures. The calculations of the parameter J begin with the critical value J_C at respective angle α.

For a fixed noncollinear angle α, with the increase of the value of J, the angular deviation between θ_{C1} and $\theta_{F2} - 180^\circ$ increases and peaks at certain J values as shown in Figs. 5(a) and 5(b). Then the angular deviation diminishes gradually with J further increasing. On the other hand, this angular deviation will also be reduced with the value of α increasing under a fixed exchange coupling constant J. Consequently, a smaller α together with a smaller J should be set in an exchange-biased system in order to gain a larger angular deviation between θ_{C1} and $\theta_{F2} - 180^\circ$, which is beneficial to the measurement of the critical angle θ_{C1}. The peaks of the angular deviation are more pronounced for a smaller noncollinear angle α, and the best value for observing the critical angle θ_{C1} is increased with α increasing. This value is approximately 2, i.e., $J \sim 2$ for $0^\circ < \alpha \leq 30^\circ$. As shown in Fig. 5(b), the maximal angular deviation between θ_{C1} and $\theta_{F2} - 180^\circ$ is only about 1.6° for $35^\circ \leq \alpha \leq 50^\circ$. In fact, it will be very difficult to observe the position of θ_{C1} in the experiment under these parameters.

4. Conclusion

In this paper, we intensively study the jump phenomenon in the angular dependence of the exchange bias with noncollinear easy axes of uniaxial and unidirectional anisotropies. It is found that complete and incomplete jump phenomena can also be observed at the intrinsic hard axis in the ADEB of the noncollinear exchange bias. The condition of the transition between complete and incomplete jump phenomena is derived by analyzing the magnetization reversal process. When the angular deviation of intrinsic hard axis from the uniaxial anisotropy axis is above the critical value 58.2826°, i.e., $\theta_{F2} - 180^\circ > 58.2826^\circ$, the complete jump phenomenon will be present in the ADEB. On the contrary, the incomplete jump phenomenon will be observed on the condition that this angular deviation is not larger than 58.2826°, i.e., $\theta_{F2} - 180^\circ \leq 58.2826^\circ$. Therefore, the complete or incomplete jump phenomenon in the ADEB is an intrinsic property of the exchange-coupled system, depending only on the location of the intrinsic hard axis, which is determined by the relative magnitude and orientation between the unidirectional anisotropy and uniaxial anisotropy.

The critical angles, at which the coercivity disappears but no jump phenomenon occurs, are also discussed in this paper. When the incomplete jump phenomenon occurs at the intrinsic hard axis, two critical angles θ_C and θ_{C1} will be observed in the ADEB, whereas only one critical angle θ_C will be shown when the complete jump phenomenon appears at the intrinsic hard axis. Based on the coherent rotation model, the physical equations about these critical angles are derived. The best parameters for observing the critical angle θ_{C1} are deduced from the relevant calculations. It is found that the exchange-biased system with a smaller noncollinear angle together with a weaker exchange coupling should be chosen to measure the critical angle θ_{C1} in the ADEB. In addition, the hysteresis loops and the modes of the magnetization reversal are also studied in this work. The magnetization reversal processes will exhibit the whole-plane rotation or half-plane rotation modes, which depends on the direction of the external field and manifests itself in the hysteresis loop of the perpendicular magnetization component.

The numerical calculations are consistent with the relevant experimental observations, which demonstrates that our approach is valid to study the ADEB for the noncollinear exchange bias. Our investigations about the types of the jump phenomena and the critical angles can explain the observed difference between different experimental results. The maximal exchange bias field as well as the maximal or minimal coercivity can be achieved artificially by tuning the external field along the orientations of the intrinsic hard axis, the critical angle, and the intrinsic easy axis. It is an important method to design or optimize the relevant magnetoresistance or spintronic devices.

References

[1] Dieny B, Speriosu V S, Parkin S S P and Gurney B A 1991 *Phys. Rev. B* **43** 1297
[2] Heim D E, Fontana R E Jr and Tsang C 1994 *IEEE Trans. Magn.* **30** 316
[3] Liu W, Liu X H, Cui W B, Gong W J and Zhang Z D 2013 *Chin. Phys. B* **22** 027104
[4] She S X, Wei D, Zheng Y, Qu B J, Ren T L, Liu X and Wei F L 2009 *Chin. Phys. Lett.* **26** 127503

[5] Shi Z, Du J and Zhou S M 2014 *Chin. Phys. B* **23** 027503
[6] Xiong Z J, Wang H Y and Ding Z J 2007 *Chin. Phys.* **16** 2123
[7] Zhang K C and Liu B G 2009 *Chin. Phys. B* **18** 3960
[8] Ambrose T, Sommer R T and Chien C L 1997 *Phys. Rev. B* **56** 8383
[9] Kim D Y, Kim C G, Kim C O, Tsunoda M and Takahashi M 2006 *J. Magn. Magn. Mater.* **304** e56
[10] Spenato D, Castel V, Pogossian S P, Dekadjevi D T and Youssef J Ben 2007 *Appl. Phys. Lett.* **91** 062515
[11] Yang P Y, Song C, Fan C B, Zeng F and Pan F 2009 *J. Appl. Phys.* **106** 013902
[12] Bai Y H, Yun G H and Bai N 2009 *J. Appl. Phys.* **106** 063919
[13] Chung S, Hoffmann A and Grimsditch M 2005 *Phys. Rev. B* **71** 214430
[14] Liedke M O, Liedke B, Keller A, Hillebrands B, Mücklich A, Facsko S and Fassbender J 2007 *Phys. Rev. B* **75** 220407
[15] BaiY H and Yun G H 2009 *Sci. China Ser. G* **52** 1885
[16] Bai Y H, Yun G H and Bai N S 2010 *J. Appl. Phys.* **107** 033905
[17] Jiménez E, Camarero J, Sort J, Nogués J and Hoffmann A 2009 *Appl. Phys. Lett.* **95** 122508
[18] McCord J, Hamann C, Schäfer R, Schultz L and Mattheis R 2008 *Phys. Rev. B* **78** 094419
[19] Jiménez E, Camarero J, Sort J, Nogués J, Hoffmann A, Dieny B and Miranda R 2009 *Phys. Rev. B* **80** 014415
[20] Dekadjevi D T, Jaouen T, Spenato D, Pogossian S P and Youssef J B 2011 *Eur. Phys. J. B* **80** 121
[21] Schafer D, Geshev J, Nicolodi S, Pereira L G, Schmidt J E and Grande P L 2008 *Appl. Phys. Lett.* **93** 042501
[22] Rodríguez-Suárez R L, Vilela-Leão L H, Bueno T, Mendes J B S, Landeros P, Rezende S M and Azevedo A 2012 *Appl. Phys. Lett.* **100** 242406
[23] Suszka A K, Idigoras O, Nikulina E, Chuvilin A and Berger A 2012 *Phys. Rev. Lett.* **109** 177205
[24] Stoner E C and Wohlfarth E P 1991 *IEEE Trans. Magn.* **27** 3475
[25] Xi H W and White R M 1999 *J. Appl. Phys.* **86** 5169
[26] Camarero J, Sort J, Hoffmann A, García-Martín J M and Dieny B 2005 *Phys. Rev. Lett.* **95** 057204
[27] Nieber S and Kronmueller H 1991 *Phys. Status Solidi B* **65** 503
[28] Thiaville A 1998 *J. Magn. Magn. Mater.* **182** 5
[29] Radu F, Westphalen A, Theis-Bröhl K and Zable H 2006 *J. Phys: Condens. Matter* **18** L29